Plasmonic-photonic arrays with aperiodic spiral order for ultra-thin film solar cells

Jacob Trevino,[1] Carlo Forestiere,[2] Giuliana Di Martino,[3] Selcuk Yerci,[2] Francesco Priolo,[3] and Luca Dal Negro[1,2,*]

[1]*Division of Materials Science & Engineering, Boston University, 15 Saint Mary's Street, Brookline, Massachusetts 02446, USA*

[2]*Department of Electrical and Computer Engineering & Photonics Center, Boston University, 8 Saint Mary's Street, Boston, Massachusetts, 02215, USA*

[3]*Dipartimento di Fisica e Astronomia, Università di Catania, Catania, Italy*

[*] *dalnegro@bu.edu*

Abstract: We report on the design, fabrication and measurement of ultra-thin film Silicon On Insulator (SOI) Schottky photo-detector cells with nanostructured plasmonic arrays, demonstrating broadband enhanced photocurrent generation using aperiodic golden angle spiral geometry. Both golden angle spiral and periodic arrays of various center-to-center particle spacing were investigated to optimize the photocurrent enhancement. The primary photocurrent enhancement region is designed for the spectral range 600nm-950nm, where photon absorption in Si is inherently poor. We demonstrate that cells coupled to spiral arrays exhibit higher photocurrent enhancement compared to optimized periodic gratings structures. The findings are supported through coupled-dipole numerical simulations of radiation diagrams and finite difference time domain simulations of enhanced absorption in Si thin-films.

OCIS codes: (250.5403) Plasmonics; (350.6050) Solar energy.

References and links

1. J. Nelson, *The Physics of Solar Cells* (Imperial College Press, 2003).
2. M. A. Green, "Third generation photovoltaics: solar cells for 2020 and beyond," Physica E **14**(1-2), 65–70 (2002).
3. H. A. Atwater and A. Polman, "Plasmonics for improved photovoltaic devices," Nat. Mater. **9**(3), 205–213 (2010).
4. K. Nakayama, K. Tanabe, and H. Atwater, "Plasmonic nanoparticle enhanced light absorption in GaAs solar cells," Appl. Phys. Lett. **93**(12), 121904 (2008).
5. K. R. Catchpole and A. Polman, "Design principles for particle plasmon enhanced solar cells," Appl. Phys. Lett. **93**(19), 191113 (2008).
6. C. Rockstuhl, S. Fahr, and F. Lederer, "Absorption enhancement in solar cells by localized plasmon polaritons," J. Appl. Phys. **104**(12), 123102 (2008).
7. V. E. Ferry, M. A. Verschuuren, H. B. T. Li, R. E. I. Schropp, H. A. Atwater, and A. Polman, "Improved red response in thin-film a-Si:H solar cells with soft-imprinted plasmonic back refelctors," Appl. Phys. Lett. **95**(18), 183503 (2009).
8. D. Song, E. Cho, G. Conibeer, C. Flynn, Y. Huang, and M. A. Green, "Structural, electrical and photovoltaic characterization of of silicon nanocrystals embedded in SiC matrix and Si nanocrystals/crystalline silicon heterojunction devices," Sol. Energy Mater. Sol. Cells **92**, 474–481 (2008).
9. M. D. Kelzenberg, S. W. Boettcher, J. A. Petykiewicz, D. B. Turner-Evans, M. C. Putnam, E. L. Warren, J. M. Spurgeon, R. M. Briggs, N. S. Lewis, and H. A. Atwater, "Enhanced absorption and carrier collection in Si wire arrays for photovoltaic applications," Nat. Mater. **9**(3), 239–244 (2010).
10. V. E. Ferry, L. A. Sweatlock, D. Pacifici, and H. A. Atwater, "Plasmonic nanostructure design for efficient light coupling into solar cells," Nano Lett. **8**(12), 4391–4397 (2008).
11. J. Zhu, C. M. Hsu, Z. Yu, S. Fan, and Y. Cui, "Nanodome solar cells with efficient light management and self-cleaning," Nano Lett. **10**(6), 1979–1984 (2010).
12. R. Biswas, J. Bhattacharya, B. Lewis, N. Chakravarty, and V. Dalal, "Enhanced nanocrystalline silicon solar cell with a photonic crystal back-reflector," Sol. Energy Mater. Sol. Cells **94**(12), 2337–2342 (2010).

#163239 - $15.00 USD Received 17 Feb 2012; accepted 5 Apr 2012; published 19 Apr 2012

13. S. B. Mallick, M. Agrawal, and P. Peumans, "Optimal light trapping in ultra-thin photonic crystal crystalline silicon solar cells," Opt. Express **18**(6), 5691–5706 (2010).
14. V. E. Ferry, M. A. Verschuuren, H. B. T. Li, E. Verhagen, R. J. Walters, R. E. I. Schropp, H. A. Atwater, and A. Polman, "Light trapping in ultrathin plasmonic solar cells," Opt. Express **18**(S2 Suppl 2), A237–A245 (2010).
15. C. Eisele, C. E. Nebel, and M. Stutzmann, "Periodic light coupler gratings in amorphous thin film solar cells," J. Appl. Phys. **89**(12), 7722 (2001).
16. C. Haase and H. Stiebig, "Thin-film silicon solar cells with efficient periodic light trapping texture," Appl. Phys. Lett. **91**(6), 061116 (2007).
17. D. Shir, J. Yoon, D. Chanda, J. H. Ryu, and J. A. Rogers, "Performance of ultrathin silicon solar microcells with nanostructures of relief formed by soft imprint lithography for broad band absorption enhancement," Nano Lett. **10**(8), 3041–3046 (2010).
18. R. H. Franken, R. L. Stolk, H. Li, C. H. M. van der Werf, J. K. Rath, and R. E. I. Schropp, "Understanding light trapping by light scattering textured back electrodes in thin film n-i-p-type silicon solar cells," J. Appl. Phys. **102**(1), 014503 (2007).
19. G. Yue, L. Sivec, J. M. Owens, B. Yan, J. Yang, and S. Guha, "Optimization of back reflector for high efficiency hydrogenated nano-crystalline silicon solar cells," Appl. Phys. Lett. **95**(26), 263501 (2009).
20. H. R. Stuart and D. G. Hall, "Island size effects in nanoparticle-enhanced photodetectors," Appl. Phys. Lett. **73**(26), 3815–3817 (1998).
21. F. J. Beck, A. Polman, and K. R. Catchpole, "Tunable light trapping for solar cells using localized surface plasmons," J. Appl. Phys. **105**(11), 114310 (2009).
22. K. Nakayama, K. Tanabe, and H. A. Atwater, "Plasmonic nanoparticle enhanced light absorption in GaAs solar cells," Appl. Phys. Lett. **93**(12), 121904 (2008).
23. A. E. Ostfeld and D. Pacifici, "Plasmonic concentrators for enhanced light absorption in ultrathin film organic photovoltaics," Appl. Phys. Lett. **98**(11), 113112 (2011).
24. V. E. Ferry, M. A. Verschuuren, M. C. Lare, R. E. I. Schropp, H. A. Atwater, and A. Polman, "Optimized spatial correlations for broadband light trapping nanopatterns in high efficiency ultrathin film a-Si:H solar cells," Nano Lett. **11**(10), 4239–4245 (2011).
25. J. A. Adam, *A Mathematical Nature Walk* (Princeton University Press, 2009).
26. J. Trevino, H. Cao, and L. Dal Negro, "Circularly symmetric light scattering from nanoplasmonic spirals," Nano Lett. **11**(5), 2008–2016 (2011).
27. E. Macia, *Aperiodic Structures in Condensed Matter: Fundamentals and Applications* (CRC Press Taylor & Francis, 2009).
28. M. Naylor, "Golden, $\sqrt{2}$, and π flowers: a spiral story," Math. Mag. **75**, 163–172 (2002).
29. G. J. Mitchison, "Phyllotaxis and the fibonacci series," Science **196**(4287), 270–275 (1977).
30. C. Janot, *Quasicrystals: A Primer* (Clarendon Press, 1992).
31. C. Forestiere, G. Miano, G. Rubinacci, and L. Dal Negro, "Role of aperiodic order in the spectral, localization, and scaling properties of plasmon modes for the design of nanoparticles arrays," Phys. Rev. B **79**(8), 085404 (2009).
32. J. Trevino, S. F. Liew, H. Noh, H. Cao, and L. Dal Negro, "Geometrical structure, multifractal spectra and localized optical modes of aperiodic Vogel spirals," Opt. Express **20**(3), 3015–3033 (2012).
33. S. F. Liew, H. Noh, J. Trevino, L. D. Negro, and H. Cao, "Localized photonic band edge modes and orbital angular momenta of light in a golden-angle spiral," Opt. Express **19**(24), 23631–23642 (2011).
34. M. E. Pollard and G. J. Parker, "Low-contrast bandgaps of a planar parabolic spiral lattice," Opt. Lett. **34**(18), 2805–2807 (2009).
35. C. Forestiere, G. Miano, S. V. Boriskina, and L. Dal Negro, "The role of nanoparticle shapes and deterministic aperiodicity for the design of nanoplasmonic arrays," Opt. Express **17**(12), 9648–9661 (2009).
36. C. Forestiere, G. F. Walsh, G. Miano, and L. Dal Negro, "Nanoplasmonics of prime number arrays," Opt. Express **17**(26), 24288–24303 (2009).
37. P. B. Johnson and R. W. Christy, "Optical constants of the noble metals," Phys. Rev. B Condens. Matter **6**(12), 4370–4379 (1972).
38. C. F. Bohren and D. R. Huffman, *Absorption and Scattering of Light by Small Particles* (Wiley, 2004).
39. S. Y. Lee, C. Forestiere, A. J. Pasquale, J. Trevino, G. Walsh, P. Galli, M. Romagnoli, and L. Dal Negro, "Plasmon-enhanced structural coloration of metal films with isotropic Pinwheel nanoparticle arrays," Opt. Express **19**(24), 23818–23830 (2011).
40. Lumerical FDTD Solutions, *www.lumerical.com*
41. A. Taflove and S. C. Hagness, *Computational Electrodynamics: The Finite-Difference Time-Domain Method. 3rd edn.* (Artech House, 2005).
42. E. D. Palik, *Handbook of Optical Constants of Solids* (Academic Press, 1997).
43. S. Mokkapati, F. J. Beck, R. de Waele, A. Polman, and K. R. Catchpole, "Resonant nano-antennas for light trapping in plasmonic solar cells," J. Phys. D Appl. Phys. **44**(18), 185101 (2011).
44. S. Pillai, K. R. Catchpole, T. Trupke, and M. A. Green, "Surface plasmon enhanced silicon solar cells," J. Appl. Phys. **101**(9), 093105 (2007).

#163239 - $15.00 USD Received 17 Feb 2012; accepted 5 Apr 2012; published 19 Apr 2012

1. Introduction

The current solar cell market is predominantly based on crystalline silicon (c-Si) wafers with absorbing layer thickness in-between 100μm-300μm to guarantee complete light absorption and effective carrier collection. However, the increasing materials fabrication costs (i.e. highly pure c-Si) and the growing efficiency demand of the solar industry have both motivated a reduction of the active cell thickness. This has typically been accomplished by using thin-films of non-crystalline Si (amorphous or poly-crystalline) [1–7] and nanocrystalline Si (Si-ncs) structures [8]. These materials can be fabricated with strongly reduced thermal budgets, costs and with much larger volumes compared to traditional Si wafers. However, their shorter diffusion lengths (limited by defects and grain boundaries) restrict the active cell thicknesses to a few hundreds of nanometers, severely decreasing the probability of photon absorption. This has recently motivated the search for advanced photon recycling and light-trapping schemes capable of increasing the optical paths of photons, and therefore the absorption probability, in ultra-thin film solar cells (< 200 nm-thick) [1,7].

Very promising approaches have been developed including the incorporation of metal-dielectric nanostructures into or atop ultra-thin film solar cells for a more efficient coupling to the incident solar radiation or to achieve resonant enhancement of absorption cross sections. Engineered nanostructures for enhanced absorption have recently been investigated in several different configurations, including nanoparticles, nanowires, photonic crystals, and random texturing [1,9–19]. In particular, recent studies have shown that metal nanostructures can lead to effective light trapping into thin-film solar cells improving the overall efficiency due to the enhancement of optical cross sections associated to the excitation of Localized Surface Plasmon modes (LSPs) [1,14]. One commonly utilized geometry consists of the fabrication of metallic nanoparticles on the front surface of the absorbing cell structure. When the nanoparticle shapes are correctly designed, incident light is preferentially scattered into the thin-film absorbing Si layer over an increased angular range, effectively enhancing the material absorption [20–22]. This plasmonic-enhanced light absorption effect has been demonstrated using periodic arrays of gold (Au) or silver (Ag) nanoparticles, which give rise to best enhancement in the spectral regions where evanescent diffraction grating orders spectrally overlap the broader LSP resonances characteristic of metallic nanoparticles. However, polarization sensitivity and the narrow frequency range for effective photonic-plasmonic coupling in periodic grating structures inherently limit these approaches. In order to broaden the spectral region of enhancement, it is crucial to engineer aperiodic nanoparticle arrays with a higher density of spatial frequencies without resorting to uncontrollable random systems, which have only limited engineering appeal. To overcome these limitations, recent studies have proposed to utilize plasmonic arrays with aperiodic quasicrystal structures, such as Penrose lattices, which exhibit non-crystallographic rotational symmetries [23,24]. Such arrays, by virtue of their higher degree of rotational symmetry as compared to traditional periodic structures, give rise to enhanced scattering along multiple directions and over a broader wavelength range.

In this study, we engineer deterministic aperiodic arrays with golden angle spiral (GA spiral) geometry [25], which feature nearly continuous azimuthal symmetry in Fourier space, leading to planar omnidirectional and polarization-insensitive light trapping into thin-film solar cells. We have recently demonstrated that plasmonic aperiodic spirals support distinctive scattering resonances carrying orbital angular momentum and produce polarization-insensitive diffraction properties across a broad spectral range [26].

Leveraging these unique aspects of nanoplasmonic aperiodic spirals, in this study we design, fabricate, and characterize the absorption and photocurrent enhancement of periodic and GA spiral arrays of Au nanoparticle fabricated atop a thin-film Schottky photo-detector structure. In particular, we engineer the spatial frequencies of GA spiral arrays to obtain large-angle and broadband light scattering and experimentally demonstrate that these novel

#163239 - $15.00 USD Received 17 Feb 2012; accepted 5 Apr 2012; published 19 Apr 2012

plasmonic structures produce larger photocurrent enhancement in the 600nm-950nm spectral range compared to optimized nanoparticle gratings. Our experimental results are supported by calculations of radiation diagrams based on the Coupled Dipole Approximation (CDA) and by absorption enhancement numerical analysis based on three-dimensional (3D) Finite Difference Time Domain (FDTD) simulations.

2. Plasmon-enhanced large-angle scattering in GA spiral arrays

GA spiral arrays are obtained by a simple generation rule, expressed in polar coordinates r and θ, first proposed by Vogel in order to approximate the complex arrangements of florets in the sunflower head in two spatial dimensions [25,27–29]:

$$\begin{cases} r = a\sqrt{n} \\ \theta = n\alpha \end{cases} \quad (1)$$

where $n = 0,1,2,\ldots$ is an integer, a is a constant scaling factor and α is known as the divergence angle. The angle α gives the constant aperture between adjacent position vectors $r(n)$ and $r(n + 1)$ of particles in the array. For the GA spiral, $\alpha \approx 137.508°$ is an irrational number known as the "golden angle". The golden angle is the angle that divides a full rotation according to the golden ratio, and can be expressed as $\alpha = 360/\varphi^2$, where $\varphi = (1 + \sqrt{5})/2 \approx 1.618$ is the golden number. A generated GA spiral array is shown in Fig. 1(a) for $n = 1500$ particles.

Figure 1(b) displays the two-dimensional (2D) reciprocal space vectors of the GA spiral array, which are obtained by the amplitude of the Discrete Fourier Transform (DFT) of the array. Due to the aperiodic nature of the GA spiral, periodic Brillouin zones cannot be rigorously defined in reciprocal space. The reciprocal space structure shown in Fig. 1(b) is instead restricted to spatial frequencies within the compact interval $\pm 1/\Delta$, with Δ being the average inter-particle separation [30,31]. Since the golden angle is an irrational number, the GA spiral lacks both translational and rotational symmetry. Accordingly, its spatial Fourier spectrum does not exhibit well-defined Bragg peaks, but rather possesses a diffuse character with a high degree of rotational symmetry (i.e., scattering ring) due to the array's large statistical isotropy [26,32,33]. The GA spiral's distinct scattering ring shown in Fig. 1(b) corresponds to the dominant spatial frequencies of the structure [26,34]. It has previously been shown that the position of the scattering ring in a GA spiral scales approximately one-to-one with the average center-to-center interparticle separation in the array [26,34]. This simple linear scaling law is critical to engineering the spectral location of planar omnidirectional diffraction in GA spirals for increased photonic-plasmonic coupling. A simple scalar Fourier optics picture already suggests that polarization-insensitive large-angle scattering of incident radiation should occur in GA spiral arrays at frequencies matching the radial position of the scattering ring in reciprocal space [26].

#163239 - $15.00 USD Received 17 Feb 2012; accepted 5 Apr 2012; published 19 Apr 2012

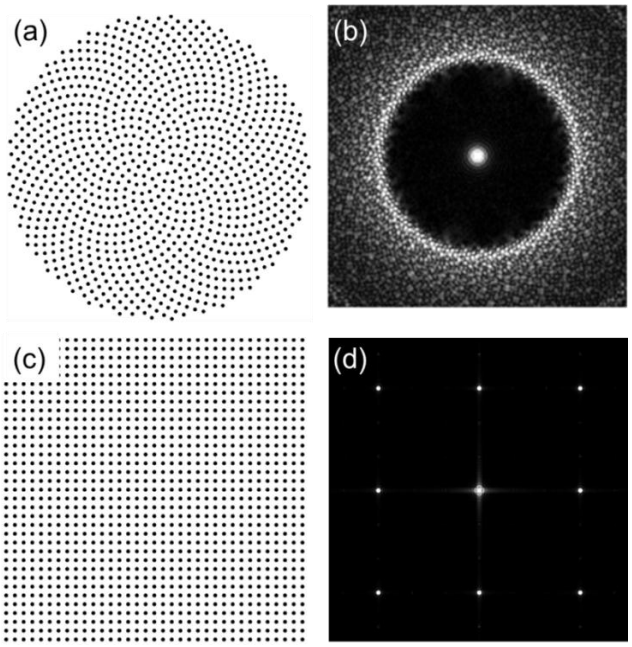

Fig. 1. (a) Periodic array of particles, N = 1225 (b) Calculated spatial Fourier spectrum of periodic array. (c) GA Spiral array with N = 1500 particles. (d) Calculated spatial Fourier spectrum of the GA spiral.

We will now discuss in more detail the relation between the spatial Fourier spectrum of GA arrays of Au nanoparticles and the large angular distribution of scattered radiation in the forward scattering hemisphere. This will be accomplished by rigorously calculating the angular radiation diagrams within the Coupled Dipole Approximation (CDA). In our formulation [31], the numerical method considers the particles of the array as ellipsoidal particles described by a single electric dipole contribution whose polarizability is a function of the ellipsoidal axis. The CDA is particularly suited to efficiently treat large-scale plasmonic systems made of small and well separated nanoparticles, and it has been previously validated against semi-analytical multiple scattering methods [35] used to describe complex nanoparticle arrangements [36]. In this paper, all the calculations are performed assuming Au nanoparticles with metallic dispersion modeled according to Johnson-Christy data [37]. All the nanoparticles were modeled by oblate spheroids with 100 nm diameter and a height of 30 nm. Moreover, the arrays are embedded in Si and are excited by a linearly polarized plane wave normally incident on the array.

The parameter of interest for the understanding of angular scattering in complex plasmonic arrays is the differential scattering cross section [38,39], which describes the angular distribution of electromagnetic power density scattered at a given wavelength within a unit solid angle centered around an angular direction (ϑ, φ) per unit incident irradiance. In the case of arrays composed of dispersive metal nanoparticles, the power scattered from a particular structure is in general a function of both the geometrical parameters of the array and the wavelength of the incident radiation. Full information on angular scattering is thus captured by calculating the averaged differential scattering cross section, where the average is performed on the azimuthal angle φ and the scattered intensity is normalized to the maximum value (i.e., forward scattering peak). By plotting the azimuthally averaged differential scattering cross section versus the inclination angle, we obtain the radiation diagrams of the arrays. In Figs. 2(a,b) we show the calculated radiation diagrams for periodic and GA arrays

#163239 - $15.00 USD Received 17 Feb 2012; accepted 5 Apr 2012; published 19 Apr 2012

at three different wavelengths λ_B = 480nm, λ_G = 550nm and λ_R = 610nm (i.e corresponding to the blue, green, and red colors), respectively.

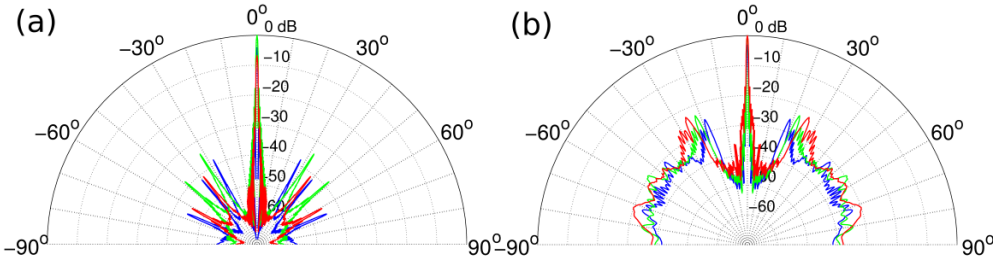

Fig. 2. Calculated radiation diagrams as a function of the inclination angle (Theta) for a periodic array with N = 3505 (a) and a GA spiral with N = 1810 (b) for three different wavelengths, namely 480nm (Blue), 520nm (Green), and 650nm (Red). The periodic array has a lattice spacing of 300 nm, the GA spiral features an averaged minimum inter-particle separation of 420nm. (The interparticle separations in both cases results from the experimental optimization performed in section 5)

The radiation diagrams are plotted in dB scale for a periodic array (Fig. 2a) and a GA spiral (Fig. 2b) of the same linear dimension D = 20μm. The periodic array contains N = 3505 nanoparticles with 300 nm lattice spacing, while the equivalent-size GA spiral has N = 1810 with 420 nm averaged minimum inter-particle separation. The results in Fig. 2(a) illustrate how the radiation diagram of the periodic nanoparticle array is dominated by coherent interactions (Bragg scattering) along certain well-defined scattering directions corresponding to the grating orders of the grating. On the other hand, the angular scattering of GA arrays (Fig. 2b) is significantly broadened at large angles (i.e. >30°) for all the investigated wavelengths, demonstrating the large-angle scattering. We expect that the phenomenon of plasmon-enhanced broadband large-angle scattering demonstrated for GA spiral arrays should redirect a larger fraction of the incident radiation into the absorbing Si substrate, thus effectively increasing the optical path of photons in the photodetector, and also enhance the coupling to LSPs in the array plane. This picture will be fully supported by the experimental results discussed in the following sections.

3. Design of the array parameters for photocurrent enhancement

In this section, we present the design of the geometrical parameters of a periodic array of nanocylinders to enhance light absorption inside the Si substrate. Numerical simulations of periodic arrays of nanoparticles were performed in order to estimate the absorption enhancement, using LUMERICAL software [40], which is a full-vector solver based on the FDTD method in 3D [41]. Unfortunately, due to the large amount of nanoparticles involved, we cannot perform a similar analysis for GA spiral structures due to their lack of translational symmetry. Therefore, GA spirals have been fabricated and tested with a large range of interparticle separations, including the ones overlapping with the optimized parameters identified here for periodic gratings. Consequently, the better performances experimentally demonstrated for GA spiral arrays in section 5 result from an experimental optimization of array parameters (i.e., interparticle separation) and those results should not be regarded as the theoretical limit of absorption enhancement achievable in Si with GA spiral arrays.

In the case of periodic arrays, the modeling of the plasmon-enhanced photodetector is obtained by considering the three-dimensional unit cell shown in Fig. 3(a). This cell is composed of a silicon substrate in air with a cylindrical Au nanoparticle directly on top. Periodic boundary conditions have been imposed on the lateral sides of the simulation box (blue dashed lines) while perfect matched layer (PML) boundary conditions were used on the top and at the bottom sides (red dashed lines). The nano-cylinder dimensions have been optimized with a 100 nm radius and 30 nm thickness, using realistic dispersion data for Au

#163239 - $15.00 USD
Received 17 Feb 2012; accepted 5 Apr 2012; published 19 Apr 2012

[42]. The device is excited from the air side by a linearly polarized plane wave propagating at normal incidence. The absorption of light inside the metallic nanoparticles is obtained by calculating the net power flux through a closed box surrounding the particle in Fig. 3(a) [43]. On the other hand, the absorption of light in the Si substrate was determined by the difference between the input and output power flows in a 50 nm-thick absorbing layer (black dashed lines). The net absorption enhancement due to the presence of the metal nanoparticle array is finally calculated by dividing the fraction of absorbed light into the 50nm-thick silicon substrate in the presence of the plasmonic particles and the absorption into the silicon layer in the absence of the plasmonic particles.

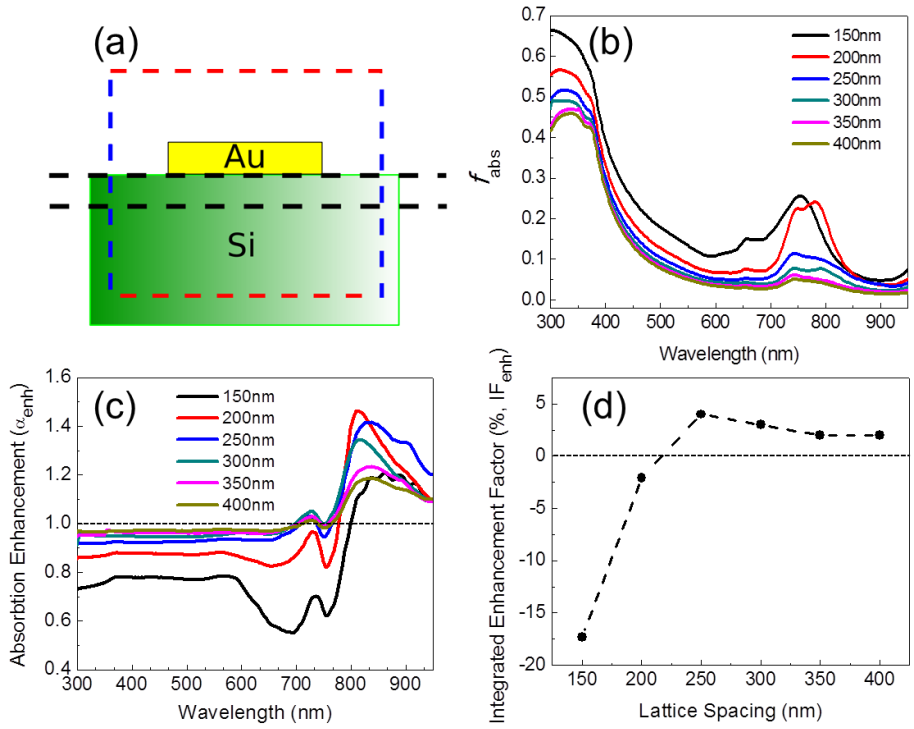

Fig. 3. (a) Schematic cross section (not to scale) of the performed FDTD simulations. The red and blue dashed lines indicate the limits of the simulation box where PML boundary conditions and periodic boundary conditions are enforced, respectively. The black dashed lines are the monitors where power fluxes are calculated. (b) Fraction of the incident power absorbed into a periodic array of gold nano-cylinders (D = 100nm, h = 30nm) and on a 50nm tick Silicon substrate, calculated with FDTD. Predicted absorption enhancement within a 50nm tick Si substrate due to a periodic array of gold nano-cylinders (D = 100nm, h = 30nm) with respect to the bare substrate (c) and the correspondent integrated enhancement factor (d).

In Fig. 3(b) we show the fraction f_{abs} of the incident power absorbed, as a function of wavelength, everywhere inside the photodetector (i.e., in the Si layer and inside the metal particles) for several values of lattice spacing. This absorbed power fraction features a distinct resonance in the spectral region around ~700nm, which originates from the excitation of LSPs in the arrays of nanocylinders. As we decrease the lattice spacing, we can observe that f_{abs} increases. In particular, for very short lattice spacings, i.e. 150, 200, we appreciate a sharp increase in f_{abs} due to the significant contribution of metallic absorption losses expected for high-density arrays. Therefore, in order to identify the respective roles of metallic losses versus dielectric absorption, we show in Fig. 3(c) the absorption enhancement α_{enh} limited to the 50nm-thick Si layer calculated in the presence/absence of the periodic array of gold

#163239 - $15.00 USD
Received 17 Feb 2012; accepted 5 Apr 2012; published 19 Apr 2012

nanocylinders. This enhancement, restricted to the Si absorbing region, is the most relevant parameter for the photodetector design. We can now notice in Fig. 3(c) that, for any value of lattice spacing, there exist two separate regimes of enhancement. In particular, for wavelengths shorter than the LSP resonance λ<700nm, the plasmonic nanoparticle array degrades the absorption efficiency compared to the one of a bare Si substrate (i.e., without nanoparticles) due to significant absorption losses inside the metallic particles. On the other hand, for wavelengths that are longer than the LSP resonance, a significant absorption enhancement in the Si layer can be obtained. In particular, at the shortest lattice spacing a = 150 nm, we found a very significant absorption degradation (i.e., α_{enh} less than one) in the short wavelength regime compared to the base Si case, since a large fraction of the incident power is absorbed inside the metal that covers in this case 35% of the silicon surface. On the other hand, a small value of α_{enh} is achieved for wavelengths longer than the LSP resonance. As we increase the interparticle spacing to a = 200 nm, α_{enh} features the highest peak among all the investigated cases. However, since the metal filling fraction is still high (20%), the absorption is still significantly decreased with respect to the bare Si substrate at shorter wavelengths. Therefore, a careful tradeoff between metal losses at short wavelengths and absorption enhancement at longer wavelengths must be obtained. We have found that the array with a = 250nm provides the best solution, as we can appreciate by considering the integrated absorption enhancement factor IF_{enh}, shown in Fig. 3(d). The IF_{enh} is defined as the average absorption enhancement ratio between λ_{min} = 300 nm and λ_{max} = 950nm, namely:

$$IF_{enh} = \frac{1}{(\lambda_{max} - \lambda_{min})} \int_{\lambda_{min}}^{\lambda_{max}} (\alpha_{enh} - 1)\, d\lambda \qquad (2)$$

As we further increase the lattice spacing in the array, we see in Figs. 3(c,d) that the absorption enhancement converges to one for wavelengths shorter than the LSP resonance, and it steadily decreases for wavelengths longer than the LSP resonance, reducing the corresponding IF_{enh}.

4. Device fabrication

To explore the potential of the GA spiral geometry for enhancing absorption and photocurrent in ultra-thin film solar cells, we have fabricated GA spirals and periodic Au nanoparticle arrays onto a thin-film stack that mimics a solar cell device. Representative scanning electron micrographs (SEM) of fabricated periodic and GA spiral Au nanoparticle arrays on Si are shown in Figs. 4(a,b), respectively.

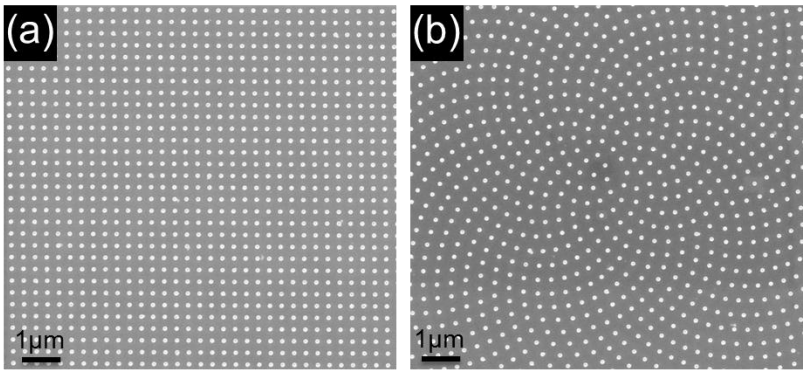

Fig. 4. Representative SEM micrographs of a (a) periodic and (b) GA Spiral array of Au nanoparticles with lattice spacing 300nm and average center to center spacing of 425nm respectively. The cylindrical particle diameters are 100nm, while the entire array geometry has a 100μm circular diameter.

#163239 - $15.00 USD Received 17 Feb 2012; accepted 5 Apr 2012; published 19 Apr 2012

We quantified the light absorption enhancement in the samples using the reflection-based technique discussed in [16] for the characterization of ultra-thin films organic solar cells. Since this experimental technique requires an optically transparent and highly reflective substrate in order to eliminate transmission losses, we fabricated a specific set of samples for these measurements, with cross sectional geometry shown in Fig. 5(a). In this case, a 300nm-thick reflecting aluminum (Al) film is first deposited by electron beam evaporation onto a Si chip. A 50nm-thick absorbing amorphous Si (α-Si) layer is then deposited by RF magnetron sputtering and Au nanoparticle arrays are fabricated atop using an Electron Beam Lithography (EBL) and a metallization process detailed in Ref. 26. The metallic particles are cylindrical in shape with a circular diameter of 100nm and thickness of 30nm. All arrays are fabricated within a circular frame region with identical diameter of 100μm. Finally, a 40nm-thick conductive and optically transparent indium tin oxide (ITO) film is deposited via RF magnetron sputtering. Sample reflectance measurements are performed using an un-polarized broadband light source coupled through an objective with high numerical aperture (50x, N.A. = 0.5) as shown in Fig. 5(b). The reflected light intensity is collected through the same objective and is spatially filtered to guarantee collection only from the area of a single 100nm-diameter spiral/periodic array. The spatially filtered light is then spectrally resolved through a monochromator coupled CCD detector (Ocean Optics QE65000 spectrometer). Spectral reflection measurements are performed on the patterned structure ($R_{array}(\lambda)$), on an unpatterned area of the chip ($R_{ref}(\lambda)$), as well as on a section of the same chip where only the Au reflecting layer is present ($R_{Au}(\lambda)$). The fraction of absorbed energy in the presence ($A_{array}(\lambda)$) and in the absence ($A_{ref}(\lambda)$) of the array is then calculated by the simple equations listed below.

$$\begin{cases} A_{array}(\lambda) = 1 - R_{array}(\lambda) / R_{Au}(\lambda) \\ A_{ref}(\lambda) = 1 - R_{ref}(\lambda) / R_{Au}(\lambda) \\ \alpha_{enh}(\lambda) = A_{array}(\lambda) / A_{ref}(\lambda) \end{cases} \quad (3)$$

The absorption enhancement $\alpha_{enh}(\lambda)$ is then calculated as the ratio of $A_{array}(\lambda)$ and $A_{ref}(\lambda)$, shown in Eq. (3). The experimental configuration assumes all scattered light is collected by the high N.A. objective. To ensure confidence in the measurements, we repeat the experiment under a 20x (N.A. = 0.4) objective and find our results to be consistent.

The set of samples used for photocurrent enhancement characterization were fabricated onto the surface of an SOI Schottky photodetector, as shown in the cross-section of Fig. 5(c). Device fabrication begins with a p-type silicon on insulator (SOI) substrate, possessing a top Si layer thickness of 50 nm. The Au nanoparticle arrays are fabricated using the same EBL and metallization process used to produce the samples for absorption quantification and have the same particle and array dimensions. Five 100 μm diameter arrays are fabricated in each active area (400μm x 400μm) of the photodetectors, as shown in the top-down microscopy image of a fabricated structure in Fig. 5(d). Conductive and optically transparent ITO films (40nm-thick) are finally deposited via RF magnetron sputtering followed by electron beam evaporation of 300nm-thick Al contacts. Both ITO and Al layers are defined by a standard photolithography and lift-off processes. A single chip was fabricated containing several periodic and GA spiral device cells, spanning in lattice spacing a large range between 120 and 680 nm. Adjacent to each device cell, an empty reference cell (i.e., without the particle array) is present to provide direct comparison for the enhancement estimation, as discussed in the next section.

#163239 - $15.00 USD Received 17 Feb 2012; accepted 5 Apr 2012; published 19 Apr 2012

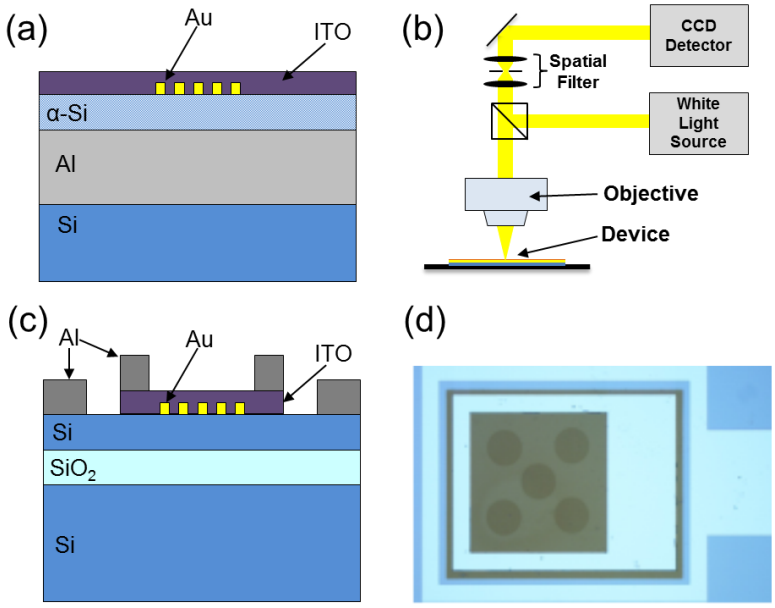

Fig. 5. (a) Device cross-section of stack used to quantify absorption enhancement. (b) Experimental reflection measurement configuration used calculate absorption enhancement. Reflection of a broadband white light source was measured by a CCD detector through excitation and collection of a 50x objective (NA = 0.5). (c) Device cross-section of the SOI Schottky photo-detector with plasmonic arrays integrated onto the absorbing surface. (d) Bright-field microscope image of the device with five 100μm diameter GA spirals integrated into the active device area.

A monochromatized broadband xenon lamp source was collimated and focused onto the active device area through a lens (f = 100 mm). Electrical probes contacting the Al pads were biased with 1 V and generated photocurrent was measured with a Keithley 2400-LV SourceMeter controlled by a computer via LabVIEW as a function of wavelength. All enhancement values calculated were derived by dividing the photocurrent spectrum for each device by its nearest neighbor empty reference cell.

5. Experimental results

In this section, we characterize the enhanced absorption and photocurrent spectra for a large number of periodic and GA spiral devices with varying interparticle separations. We will first discuss the experimental results on light absorption enhancement. To this regard, it is important to notice that the previously discussed reflection-based technique does not allow for distinction between the two absorption contributions originating from Si on one hand, and the metallic nanocylinders on the other hand. In Fig. 6(a) we plot few representative examples of experimentally measured absorption enhancement spectra obtained for a GA spirals (solid lines) and for periodic arrays (dashed lines) with varying interparticle separations (reported in the legend) ranging from 120 nm to 680 nm. The presence of a plasmon-enhanced resonance around 700nm separating two separate enhancement regimes (for $\lambda<700$nm or $\lambda>700$nm, respectively) is clearly visible in Fig. 6(a), as predicted based on the numerical simulations shown in Fig. 3(a). The absorption enhancement spectra in Fig. 6(a) are influenced by both the light absorbed in the α-Si thin film as well as the one absorbed inside the metallic nanoparticles. Therefore, as previously discussed in relation to Figs. 3(b,c), the metallic losses will dominate the total absorption at wavelengths shorter than the LSP resonance, while for longer wavelengths the absorption in the α-Si thin film can be enhanced. The total absorption enhancement spectral data shown in Fig. 6(a) follow closely the trends with respect to

#163239 - $15.00 USD
Received 17 Feb 2012; accepted 5 Apr 2012; published 19 Apr 2012

interparticle separations predicted by the numerical simulations shown in Fig. 3(b) for periodic array.

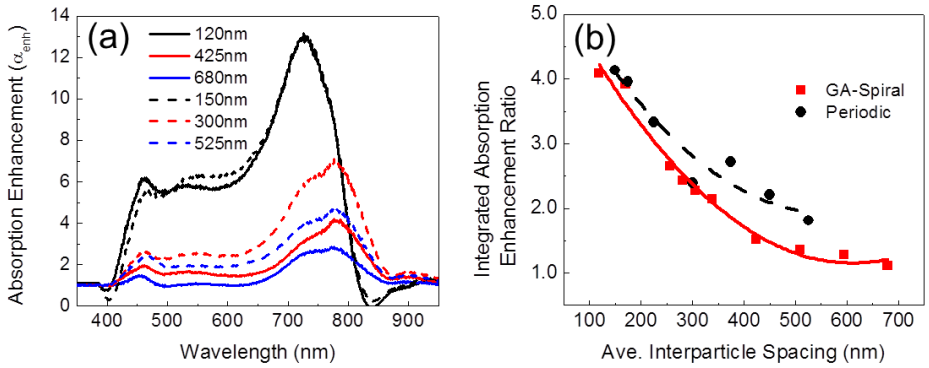

Fig. 6. (a) Experimental absorption enhancement for a GA spirals (solid lines) with average center to center spacing of 120nm, 425nm, and 680nm and periodic arrays (dashed lines) with lattice spacing of 150nm, 300nm, and 525nm. (b) Integrated absorption enhancement ratio for GA spirals (red, solid) and periodic (black, dashed) arrays of various interparticle spacing. Enhancement ratios are calculated by the ratio of the integrated measure with the nanopatterned device verses the integrated measure without nanopatterning.

In Fig. 6(b) we show the integrated absorption ratio for all the investigated arrays as a function of center-to-center particle spacing. The integrated absorption enhancement ratio is defined as the ratio between the integrated absorption spectra measured on the patterned structure and on a reference unpatterned area of the chip. We notice in Fig. 6(b) that for arrays with comparable center-to-center spacing, periodic structures always appear to produce larger values of integrated absorption enhancement. However, this result simply reflects the differences in Au nanoparticle densities for devices. In fact, for arrays of the same particle spacing, the GA spiral structures are approximately 50% less dense in metal nanoparticles than periodic structures. Therefore, as we will also confirm by direct photocurrent measurements, the integrated absorption enhancement data shown in Fig. 6(b) are dominated by the metallic losses of the more dense periodic arrays.

A definitive picture that demonstrates the full potential of the GA spiral geometry for enhancing the absorption into thin Si films can be obtained by comparing directly the photocurrent generated in periodic and GA spiral array Schottky photodetectors as a function of wavelength. Figure 7(a) and 7(b) show the measured photocurrent spectra for the best performing periodic and GA spiral photodetectors. The dashed lines are the reference photocurrent spectra measured on the unpatterned devices in the nearest reference cells, respectively. The best results were obtained for periodic arrays with 300 nm particle spacing while the best GA performances have been measured for 425 nm average interparticle separation. In Fig. 7(c) we plot the spectral photocurrent enhancement obtained by considering the ratio of the array and the corresponding reference measurements. Values below the dotted line of value one in Fig. 7(c) indicate a global reduction in photocurrent compared to an unpatterned device area. The presence of nanoplasmonic arrays was found to substantially affect the photocurrent measured in the devices across the investigated wavelength spectrum. As observed in the data in Fig. 7(a)-7(c), the patterned cells show significant photocurrent enhancements for wavelengths in the 600 nm to 950 nm region, which are around or longer than the LSP resonance wavelength measured in Fig. 6(a). On the other hand, for shorter wavelengths we observe a clear decrease in absorption compared to the reference Si cell for the periodic arrays (Fig. 6c), consistently with the predictions based on our numerical modeling (Fig. 3c). We also notice from Fig. 7(c) that the GA spiral arrays do

#163239 - $15.00 USD
Received 17 Feb 2012; accepted 5 Apr 2012; published 19 Apr 2012

not deteriorate the absorption in Si but introduce only negligible metallic losses due to the 50% reduction in array filling fraction. Since the GA spiral diffracts a larger fraction of light into high angles directions (Fig. 2) than periodic arrays, less metal particles are required to obtain comparable scattered power into the Si substrate. The maximum photocurrent enhancement of approximately a factor of 3 is measured for the GA spiral at 950 nm. This increased photocurrent results from the interplay of plasmonic-photonic effects in GA spirals, which contribute to the overall enhancement as follows: by providing better coupling of incident radiation into the thin Si layer due to photonic large angle scattering (Fig. 2); by enhancing the intensity of the nanoparticle near-fields at the Si interface owing to better LSP coupling in the plane of the array as compared to periodic structures [14,44].

We notice finally that, to varying degrees, all structures with incorporated nanoplasmonic particles feature a reduced photocurrent in the blue part of the solar spectrum below the LSP resonance, as predicted by simulations in Fig. 3. This reduction is caused by both the onset of metallic losses in the nanoparticles near the LSP resonance as well as by destructive Fano interference induced by plasmonic scattering below the surface plasmon resonances [21,22].

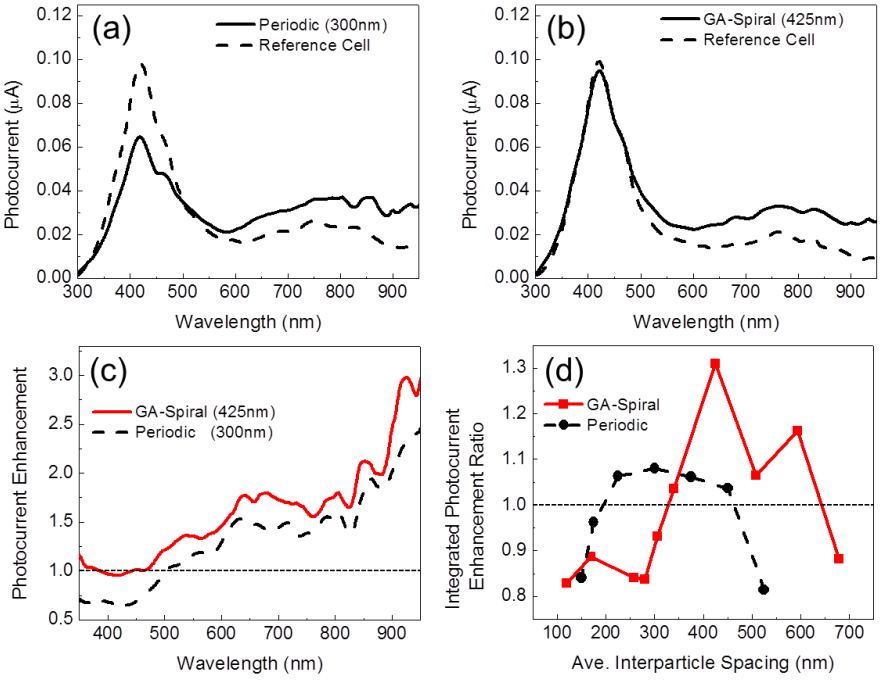

Fig. 7. (a) Periodic array photocurrent spectrum with lattice spacing of 300nm (solid) and empty neighbor reference cell (dashed). (b) Spiral array photocurrent with average center to center spacing of 425nm (solid) and empty neighbor references cells (dashed). (c) Spectral photocurrent enhancement spectra for GA spiral arrays (red, a = 425nm) and periodic arrays (black dashed, a = 300nm). (d) Integrated photocurrent enhancement ratio for GA spiral (red) and periodic (black dashed) arrays of different center to center particle spacing.

In Fig. 7(d) we show the integrated photocurrent enhancement ratio, calculated by the ratio of the integrated photocurrent spectrum of the device with and without the plasmonic arrays. The ratios falling below the dotted line indicate devices with overall reduced performance when compared against their neighboring empty reference cells. We see in Fig. 7(d) that both GA spiral and periodic arrays exhibit an optimization trend with respect to the interparticle spacing, yielding maximum integrated enhancements of 8% and 31% over reference cells, respectively. The periodic array with highest integrated enhancement

#163239 - $15.00 USD
Received 17 Feb 2012; accepted 5 Apr 2012; published 19 Apr 2012

corresponds to a lattice spacing of 300 nm, which is in good agreement with the predicted performance shown in Fig. 3(d) based on calculated absorption enhancement. The increased enhancement observed for GA spirals follows from their circular Fourier space inducing the large-angle scattering effect discussed and modeled in Fig. 2.

Finally, we remark that that observed 31% integrated enhancement measured for GA spiral arrays has been demonstrated with only 25% of the active photodetector device area covered by GA arrays (Fig. 5d). This highlights the potential for even greater enhancement in the limit of complete device area coverage using GA spirals. While this study has focused on enhancing thin-film Si Schottky photodetectors, the unique plasmonic-photonic behavior of GA spiral arrays presented here are generally scalable to other solar cell material platforms and wavelength regimes. Moreover, a large class of deterministic aperiodic spiral arrays with divergence angles different from the golden angle remains to be explored, promising even more flexibility in Fourier space while maintaining almost ideal circular symmetry in multiple scattering rings [26].

6. Conclusion

We have experimentally investigated ultra-thin (100 nm) SOI Schottky photo-detector cells coupled to GA spiral and periodic Au nanoparticle arrays for efficient light trapping. We demonstrate that photodetector devices coupled to optimized GA spiral geometry enhance the spectrally integrated photocurrent by 31%, as compared to only 8% observed in periodic arrays. The resulting enhancement has been related to the distinctive properties of GA spirals, which give rise to strong photonic high-angle scattering behavior increasing the coupling into the thin-film absorbing Si layer and the localized plasmonic resonances atop the absorbing region, at significantly reduced metallic particles densities compared to periodic array. Our results are supported by electromagnetic modeling of angular radiation diagrams and absorption enhancement spectra based on CDA and FDTD numerical simulations. This study introduces a new engineerable platform providing broadband large-angle scattering and light trapping for applications in thin-film solar cells and for photodetectors enhancement.

Acknowledgments

This work was supported by the Air Force program “Deterministic Aperiodic Structures for On-chip Nanophotonic and Nanoplasmonic Device Applications” under Award FA9550-10-1-0019. This work was also partly supported by the “Engineering structural colors in metal films” project sponsored by APIC Corporation and PhotonIC Corporation.

#163239 - $15.00 USD Received 17 Feb 2012; accepted 5 Apr 2012; published 19 Apr 2012